Growing season methane emissions from a permafrost peatland of northeast China: Observations using open-path eddy covariance method

Xueyang Yu [a, b], Changchun Song [a, *], Li Sun [a], Xianwei Wang [a], Fuxi Shi [a], Qian Cui [a, b], Wenwen Tan [a]

[a] Key Laboratory of Wetland Ecology and Environment, Northeast Institute of Geography and Agroecology, Chinese Academy of Sciences, Changchun, 130102, PR China
[b] University of Chinese Academy of Sciences, Beijing, 100049, PR China

HIGHLIGHTS

- Strict filtering criteria are applied to reveal methane emission patterns.
- Seasonal permafrost thawing is added to classical temperature response equation.
- Precipitation is likely to control inter-annual variation when permafrost exists.

ARTICLE INFO

ABSTRACT

The mid-high latitude permafrost peatlands in the Northern Hemisphere is a major natural source of methane (CH_4) to the atmosphere. Ecosystem scale CH_4 emissions from a typical permafrost peatland in the Great Hing'an Mountains were observed during the growing season of 2014 and 2015 using the open-path eddy covariance method. Relevant environmental factors such as temperature and precipitation were also collected. There was a clear diurnal variation in methane emissions in the second half of each growing season, with significantly higher emission rates in the wet sector of study area. The daily CH_4 exchange ranged from 1.8 mg CH_4 m^{-2} d^{-1} to 40.2 mg CH_4 m^{-2} d^{-1} in 2014 and ranged from −3.9 to 15.0 mg CH_4 m^{-2} d^{-1} in 2015. There were no peaks of CH_4 fluxes during the spring thawing period. However, large peaks of CH_4 emission were found in the second half of both growing seasons. The CH_4 emission after Jul 25th accounted for 77.9% of total growing season emission in 2014 and 85.9% in 2015. The total CH_4 emission during the growing season of 2014 and 2015 was approximately 1.52 g CH_4 m^{-2} and 0.71 g CH_4 m^{-2}, respectively. CH_4 fluxes during the growing seasons were significantly correlated with thawing depth ($R^2 = 0.71$, $P < 0.01$) and soil temperatures ($R^2 = 0.75$, $P < 0.01$) at 40 cm depth. An empirical equation using these two major variables was modified to estimate growing season CH_4 emissions in permafrost peatlands. Our multiyear observations indicate that the time-lagged volume of precipitation during the growing season is a key factor in interpreting locally inter-annual variations in CH_4 emissions. Our results suggested that the low temperature in the deep soil layers effectively restricts methane production and emission rates; these conditions may create significant positive feedback under global climate change.

© 2017 Elsevier Ltd. All rights reserved.

1. Introduction

Atmospheric methane (CH_4) is both a contributor and indicator of climate change and variability (Laetitia et al., 2008). On a per mole basis, the comparative impact of CH_4 on climate change is more than 25 times greater than CO_2 over a 100-year period

(Rodhe, 1990). Atmospheric CH_4 background concentrations have risen from 0.7 ppm to 1.8 ppm since the industrial revolution (IPCC, 2013), exceeding the highest annual mean concentration over the past 800,000 years (Laetitia et al., 2008).

As the largest global natural source, wetlands emit nearly 580 Tg CH_4 yr^{-1} into the atmosphere, making up more than 20% of global CH_4 emissions (Fung et al., 1991). Northern peatlands, a type of wetlands mainly distributed in boreal and subarctic areas, cover an area of 4×10^6 km^2, or approximately 3% of all land surface and 63% of all wetlands (Joosten and Clarke, 2002). Approximately 455 Pg carbon is buried in northern peatlands, amounting to one third of the global soil carbon pool and 75% of the global atmospheric carbon pool (Gorham, 1991). Approximately 6–40 Tg CH_4 yr^{-1} is released from northern peatlands, equivalent to 12% of global CH_4 emissions (Wuebbles and Hayhoe, 2002). Because of its large carbon storage capacity and the sensitivity of high-latitude ecosystems to global warming, northern peatlands have a significant influence on greenhouse gas emissions.

Methane emissions result from complex physical and biochemical processes (Bubier and Moore, 1994). Methane is released through diffusion, ebullition, and plant-mediated transport (Imelda et al., 2013; Lai, 2009). Many studies have identified mechanisms influencing methane release, such as water table, soil temperature, soil redox potential, atmospheric pressure, water vapor deficiency (Dirk et al., 2005; Kim, 2015; Metje and Frenzel, 2007; Moore and Dalva, 1993; Whiting and Chanton, 1992). Soil temperature and water table appear to be the primary factors controlling peatland CH_4 emissions (Bergman et al., 1998; Funk et al., 1994; Moore and Knowles, 1989; Suyker et al., 1996; Updegraff et al., 2001; Weiss et al., 2006). However, field observations have shown only weak correlations between CH_4 emissions and environmental factors in northern peatlands (Hommeltenberg et al., 2014; Rinne et al., 2007; Ström et al., 2012).

Northern peatlands have experienced significant climate change including increasing average temperature and precipitation. This has resulted in permafrost degradation (Hinkel and Outcalt, 1994; Schuur et al., 2008). Methane production, which is a microbial-mediated reaction, can be accelerated by higher temperature. Meanwhile, higher temperature can also increase the conductance for methane diffusion and plant-mediate transport (Hosono and Nouchi, 1997), which enhances release processes and can lead to higher methane emissions. Predicting the response of northern peatland ecosystems requires determining the dominant influencing factors and their controlling mechanisms.

Because of the complexity of production and release processes, emission rates fluctuate significantly both temporally and spatially (Hanis et al., 2015; Nykänen et al., 2003; Zhu et al., 2014). Single-parameter relationships between environmental factors and methane flux have been insufficient to predict methane emissions at variable time scales (Christensen et al., 1995; Nakano et al., 2000; Whalen and Reeburgh, 1992). Statistical methods, for example path analysis (Iwata et al., 2015; Song et al., 2015) and CRAT (Classification and Regression Tree) analysis (Nadeau et al., 2013) have been applied to evaluate the importance of different factors. However, although the factors influencing methane emissions can be ranked in order of importance, they remain difficult to quantify. This has led to significant interest in quantifying CH_4 emissions from different sources (Song et al., 2015). More in situ observations with high time resolution and large space scale are still needed.

The common chamber method has proved unsatisfactory to estimate landscape-scale methane flux (Davidson et al., 2002; Juszczak, 2013; Rochette et al., 1992). Instead, the eddy covariance (EC) method provides noninvasive continuous ecosystem greenhouse flux datasets, and has therefore been used more frequently (Aurela et al., 2009; Baldocchi et al., 2012; Baldocchi, 2003; Iwata et al., 2015; Roulet et al., 1992; Sonnentag et al., 2010). However, the EC method has limitations as it requires a relatively homogeneous location with steady atmospheric condition of adequate turbulence exchange (Aubinet et al., 2012; Rinne et al., 2007). Nighttime flux datasets are usually of low quality when turbulence exchange occurs intermittently (Gu et al., 2005). The measurement footprint therefore may extend beyond the area of interest, and gas may be stored below the layer of the gas analyzers (Lai et al., 2002; Ran et al., 2016). For now, the instrumental malfunctions and insufficient turbulence result in highly-deviated discontinuous half-hourly fluxes (Hanis et al., 2015; Kowalska et al., 2013). Moreover, data quality control and gap-filling strategies are important in evaluating long term greenhouse gas budgets (Beetz et al., 2012; Falge et al., 2001; Mcveigh et al., 2014). Further analyses on EC methane emission datasets are necessary.

This study examined growing season methane emission dynamics from an ombrotrophic peatland in the Great Hing'an Mountains, northeastern China, using open-path EC method. The study's main objectives were to: (I) explore the observational data to detect temporal and spatial patterns in methane emissions at different time scales; (II) integrate micrometeorological observations to assess the relationship between methane emission and relevant environmental factors, and (III) compare relevant research with this study's results to gain insights about methane emission variation among different sites and about the inter-annual variation of methane flux in permafrost peatlands in general.

2. Material and methods

2.1. Study area

This study was conducted in a permafrost peatland in the north of the Great Hing'an Mountains (52° 56′ 32.400″ N, 122° 51′ 23.203″ E, 473 A.S.L.) in Northeast China (Fig. 1). A branch of the Emuer River runs along the southern border of the peatland. Hydrological conditions of the peatland are mainly controlled by precipitation; no stream source was observed during this study. Soil pore water has a pH lower than 5, and the maximum active layer depth ranges from 60 cm to 80 cm in September (Wang et al., 2010).

The peatland is approximately 800 m long in the east-west direction and 250 m long in the north-south direction and surrounded on all sides by forests. It is located in the cold temperate zone with an ice-free period generally between May and October. The mean annual temperature was −3.9 °C during 1980–2009 with a mean annual precipitation of 452 mm; 203 mm of this precipitation fell in July and August. January is the coldest month, while July is the warmest. Mean air temperature in January and July (1980–2009) was −28.7 °C and 18.4 °C, respectively (Song et al., 2009).

2.2. Vegetation

Fifty percent of the peat surface is occupied by hummocks covered with continuous moss and shrubs; sedge tussocks with hollows cover the rest of the area. Deciduous shrubs (*Betula fruticosa, Vaccinium uliginosum, Salix myrtilloide*), evergreen shrubs (*Ledum palustre, Rhododendron capitatum, Chamaedaphne calyculata*), sedges (*Eriophorum vaginatum*) and moss (*Sphagnum capillifolium, Sphagnum magellanicum*) are the dominant species at the study site. Shrubs, sedges, and moss layer heights are 45–50, 30–33, and 10–12 cm, respectively. Above ground biomass (dry weight) is averagely 400–600 g m^{-2} (Meng et al., 2014; Miao et al., 2012; Wang et al., 2010). Forests of *Larix gmelinii* and *Betula platyphylla* border the site; a few trees of the same species grow in the site. The soil at the study site was a typical peat soil, with the peat
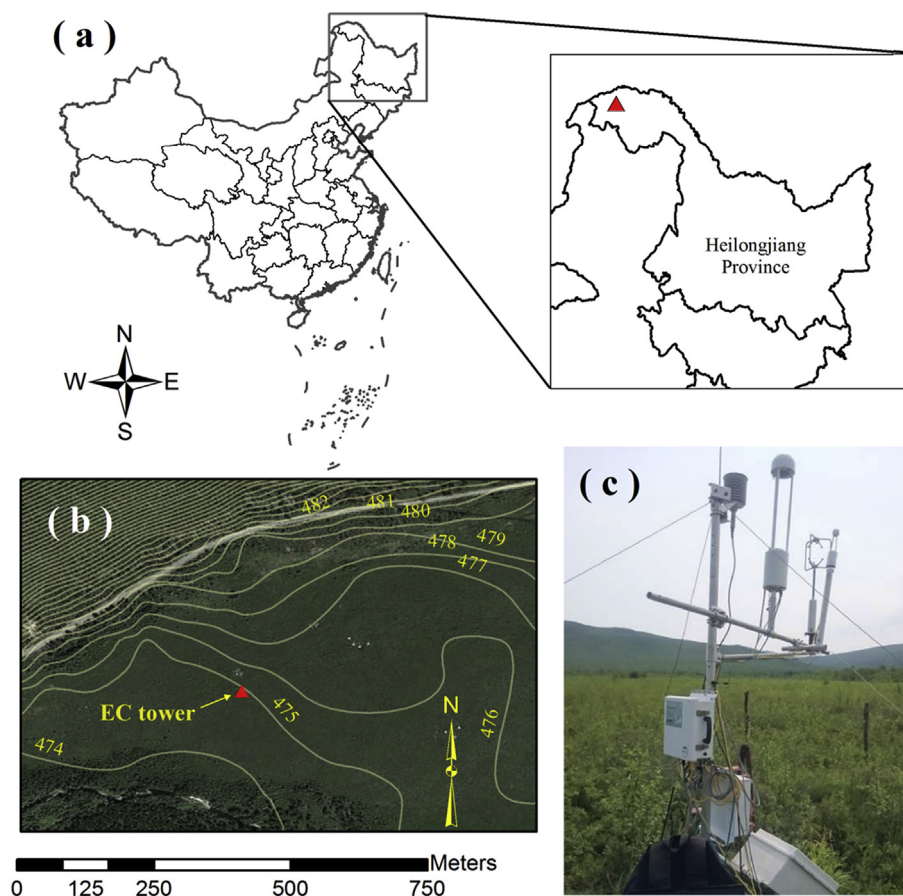
Fig. 1. (a) The location of the experiment site (red triangle) on the map of China, (b) the approximate topography around the eddy covariance tower, which is marked as a red triangle (the underlying map is obtained from Google Earth and the contour lines are calculated using the DEM data from SRTM with resolution of 90 m), (c) the field picture of the eddy covariance tower with a view towards south. (For interpretation of the references to colour in this figure legend, the reader is referred to the web version of this article.)

layer ranging from 40 cm to 60 cm.

inserting a metal rod into the peat approximately once a week.

2.3. Instrumentation

The open path EC system was established in 2014, and consisted of a three-dimensional sonic anemometer (Windmaster Pro, Gill Instruments, England), a CO_2/H_2O gas analyzer with its interface unit (LI-7500A, LI-COR Biosciences, USA), and an open-path CH_4 analyzer (LI-7700, LI-COR Biosciences, USA). The CO_2/H_2O analyzer and CH_4 analyzer were mounted at a height of 2.9 m above ground surface; they were horizontally separated from the sonic anemometer by 0.26 m and 0.72 m, respectively. All sensors were calibrated before observation.

A micrometeorological measurement system was set 50 m northwest of the EC system. It consisted of a data logger (CR1000, Campell Scientific, USA), soil temperature sensors (QT109, Campell Scientific, USA), soil moisture sensors (CS616, Campell Scientific, USA), a platinum resistance thermistor & humidity sensor (HMP 45AC, Vaisala, Finland) with a radiation shield and a precipitation gauge (S-RGB-M002, Onset Computer Corporation, USA). Soil temperature and moisture sensors were mounted at peat depths of 0.05, 0.1, 0.15, 0.2, 0.4 and 0.6 m below the surface.

EC measurements were made during the growing seasons of 2014 and 2015. Eddy covariance data were collected at 10 Hz. Supporting meteorological data were logged every minute, except for soil temperature and volumetric water content, which were logged every 15 min. Thaw depth was measured manually by

2.4. Data processing

Raw data were processed by EddyPro v6.0 (https://www.licor.com/env/products/eddy_covariance/eddypro.html). An averaging time of 30 min was selected according to an ogives function which was defined as the cumulative integral of the flux co-spectrum from the small to the large frequencies (Foken et al., 2012). An averaging period of 10 min was selected when revealing a single day's more detailed flux variation which was similar to Nadeau et al. (2013). Ogives calculated on a typical sunny afternoon (07/08/2015 13:00–17:00) led to results for an averaging period of 10 min that were not much different from 30 min. Sun et al. (2006) also found the same results in cropland.

In each averaging period, raw data quality was checked statistically (Vickers, 1997) to detect and remove data under unrealistic situations. These situations included spikes, low signal amplitude, drop-outs, and outliers. The diagnostic output of LI-7700, i.e. the relative signal strength indicator (RSSI), was used to filter out the raw CH_4 concentration data when LI-7700 was working poorly. In this study CH_4 data with RSSI lower than 20% was discarded. The angle-of-attack correction for the sonic anemometer was applied based on Nakai and Shimoyama (2012). A double rotation of the coordinate was performed to ensure that the mean vertical and cross-streamwise velocities were zero. Mean values of scalars were removed by block averaging. Time lag caused by sensor separation

was corrected using a covariance maximization procedure. High frequency loss resulting from systemic setup such as sensor separation and inadequate sensor frequency response, was corrected according to Moncrieff et al. (1997). Low frequency spectral loss due to finite averaging time and detrending was implemented following Moncrieff et al. (2004). The true cospectra estimation was performed by using analytical cospectra formulations (Moore, 1986). In each average period, the low-pass and high-pass transfer functions were specified to evaluate response losses at different frequencies. Then flux attenuation was estimated by converting the observed flux cospectrum to the true flux cospectrum. Under most (79.3%) circumstances, less than 20.0% were added to the calculated flux via spectroscopic correction while on average 19.9% were added to calculated flux. Air density changes during the averaging periods were compensated using WPL correction (Webb et al., 1980), spectroscopic correction for LI-7700 CH_4 analyzer was also applied along with the WPL correlation to compensate spectroscopic effects in every averaging period.

Half-hourly fluxes during sensor malfunctions were removed first. In 2014, the eddy covariance observation period was from June 5th to October 8th and a total of 3634 half-hourly fluxes were obtained, which led to a data coverage of 60.6%. In 2015, the observation period was from May 11th to October 13th. A total of 5911 half-hourly fluxes were obtained, which led to a data coverage of 79.6%. Previous studies in this region (Meng et al., 2014; Miao et al., 2012) indicated that methane emissions were unlikely to be outside the range of $-0.04-0.20$ μmol CH_4 m^{-2} s^{-1}, equivalent to $-2.30-11.52$ mg CH_4 m^{-2} h^{-1}. The unit of CH_4 flux "mg CH_4 m^{-2} h^{-1}" is simplified as "mg m^{-2} h^{-1}" and "mg CH_4 m^{-2} d^{-1}" is simplified as "mg m^{-2} d^{-1}" hereafter. It is the same with the unit of CH_4 seasonal emission that "g CH_4 m^{-2}" is simplified as "g m^{-2}". Therefore, fluxes outside this range were discarded. Nighttime CO_2 fluxes during a two-month period (2014/7—2014/8) were chosen to determine the friction velocity (u*) threshold (Fig. 2) because CH_4 emissions did not exhibited great variation (Gu et al., 2005). When the number of grouped nighttime fluxes was small, the average flux was easily influenced by extreme points, which led to the high average flux when u* is low. This phenomenon was also discussed by Gu et al. (2005). Therefore, the u* range of $0-0.02$ m s^{-1} (equal to 0.4% of all points) was eliminated from analysis as was the range of u* > 0.25 m s^{-1} (equal to 2.8% of all points). High variation in the average of the grouped flux was found when u* was above 0.16 m s^{-1} (grey rectangle in Fig. 2). This was also caused by the limited flux numbers in each average group. Despite the drawbacks, the average flux increased along with the u* until it tended to level off and be independent of the u* at around 0.1 m s^{-1}. Besides, the

nighttime CO_2 fluxes were randomly distributed along with air temperature ($R^2 = 0.05$) which meant nighttime CO_2 fluxes is independent of air temperature. Therefore the u* threshold was determined to be 0.1 m s^{-1}. Then the fluxes with u* < 0.10 m s^{-1} were removed because they reflected insufficient turbulence (Iwata et al., 2015). The total coverage of the initial filtered fluxes in 2014 and 2015 was 43.2% and 62.9%, respectively.

However, high variations in methane emissions still exist in this filtered eddy covariance dataset which could potentially conceal the relationship between methane emissions and controlling factors. To reveal methane emission patterns and the internal relationships between methane fluxes and controlling factors, several strict filtering criteria such as footprint estimations and stationary test were applied. These ensured that the most ideal observation conditions were satisfied and that the most accurate methane fluxes were obtained. Footprint estimations were carried out based on Kljun et al. (2004) and flux quality was determined based on Foken et al. (2004) using a 1—9 flag system (flag 1 was of best quality while 9 of the worst). The fluxes for seasonal emission estimates were filtered using acceptance criteria which was 90% fetch did not overlap the non-peatland area. Furthermore, to avoid the disturbance around eddy tower, fluxes with a maximum contribution at a distance of less than 10 m were also removed. Then, only fluxes with good quality flag (1 and 2) based on Foken et al. (2012) 1—9 system were retained. In each period (defined in Chapter 3.1), flux outliers that exceed three times the standard deviations were discarded. These final screened data covered 18.9% of all observation periods in 2014 and 26.8% in 2015.

2.5. Data utilization

Fig. 3a and Fig. 3b show preliminary filtered half-hourly fluxes and strictly filtered half-hourly fluxes, respectively. Within each averaging period, the calculated footprint may extend beyond the area of interest, or environmental conditions may change significantly. Therefore, half-hourly fluxes were still scattered though they were filtered using absolute limits and friction velocity thresholds. Spikes were effectively detected and removed through the strictly filtering using footprint estimation and turbulence stability evaluation. However, the number of accepted fluxes also concurrently decreased (Fig. 3b). Although the numbers of half-hourly fluxes observations decreased as a consequence, the data quality was improved. July 25th was subjectively selected to divide the growing season into two periods (periods I and II) as methane emission patterns differed significantly between the two periods.

The strictly filtered fluxes were used to reveal diurnal and spatial variations because of their higher quality and accuracy. The correlations between flux and the controlling factors were detected using these strictly filtered fluxes as well. However, when converting half-hourly fluxes to daily fluxes then estimating seasonal methane emission, not enough daily fluxes were obtained using the strictly filtered fluxes in the growing season of 2014. This resulted in an overestimation when estimating seasonal budgets. Under this condition, the initial filtered fluxes were utilized during both growing seasons. Seasonal budget was calculated separately using the initial and strictly filtered data of 2015. The difference of the seasonal budget estimates was less than 1%.

2.6. Seasonal budget estimation

After strictly filtering, limited but high quality half-hourly fluxes were obtained. This helped to gain a better understanding of the relationship between fluxes and controlling factors. However, as discussed below in Section 3, methane fluxes exhibited great temporal and spatial variations, thus it is difficult and inaccurate to
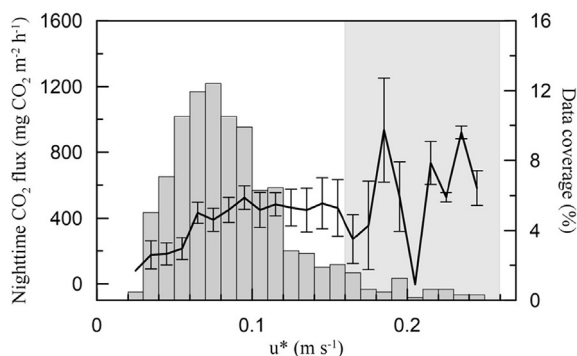
Fig. 2. The relationship between the nighttime CO_2 flux (+/− s. e.) and the friction velocity (u*). The bars represent the coverage of methane fluxes in 0.02 m s^{-1} increments. The group with u* > 0.25 m s^{-1} and standard errors exceeding axes range were not displayed in plot.
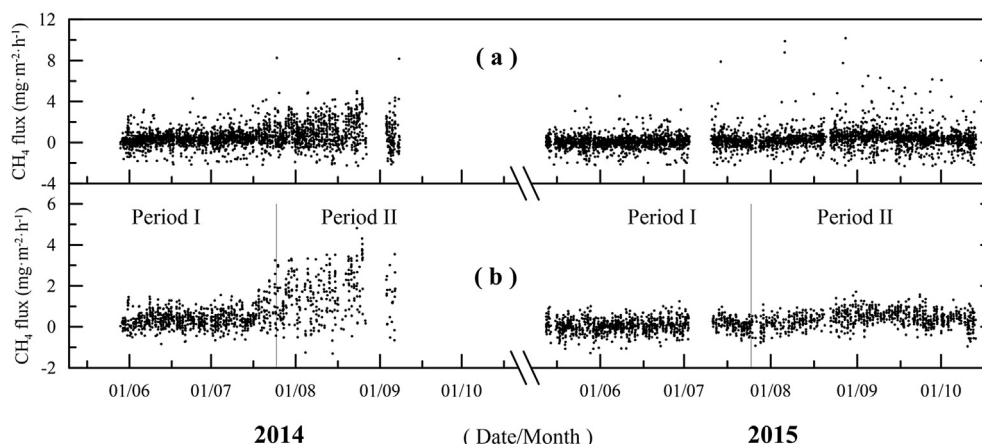
Fig. 3. (a) Time series of the half-hourly CH$_4$ fluxes; (b) time series of the strictly filtered half-hourly CH$_4$ fluxes.

validate a predicting equation directly using half-hourly flux data. Instead, daily methane fluxes were used to quantify the relationship between CH$_4$ emissions and environmental controlling factors.

Since nighttime fluxes varied greatly and did not meet the filtering criteria, days with more than 12 half-hourly daytime fluxes after preliminary filtering were used to calculate daily emissions. However, if daily flux was estimated using the average or the median value of the filtered data for a single day, an overestimation occurred when nighttime emission was not as high as daytime emission. Therefore, the nighttime fluxes (from 18:00 to 6:00 a.m. next day) were compensated for by the overall median methane emission within each period (2014: Period I - 0.1500 mg m^{-2} h^{-1}, Period II - −0.0262 mg m^{-2} h^{-1}; 2015: Period I - 0.0365 mg m^{-2} h^{-1}, Period II - 0.2828 mg m^{-2} h^{-1}). The daytime (from 6:00 a.m. to 18:00) flux was calculated using the median value within this period. The daily emission was then calculated by adding the daytime emission and the nighttime emission. The relationship between daily CH$_4$ fluxes and environmental factors in each independent growing season were then examined. Seasonal budget was estimated according to a promoted statistical model validated in Section 3.4.5.

3. Results and discussion

3.1. Environmental conditions

Mean air temperature during the 2014 and 2015 growing seasons was 12.75 °C and 13.00 °C, respectively. In May and June, mean air temperatures were higher in 2014 (11.54 °C for May and 16.07 °C for June) than in 2015 (9.08 °C for May and 14.38 °C for June). The mean air temperature of all other months was lower in 2014 than in 2015. Total precipitation for the growing seasons of 2014 and 2015 was 236.9 and 333.0 mm, respectively, lower than the 30-year mean precipitation of 385.4 mm.

A heavy rainfall event occurred from July 25 to 27, 2015 with a total amount of 92.8 mm (Fig. 4a). The heavy rainfall event corresponded with abrupt change point of deep layer temperature curves, indicating that rainfall in mid-summer accelerated permafrost thawing. This finding was consistent with Kokelj et al. (2015), who found that precipitation could affect ice thawing. Only the temperature of the upper soil layer (0−15 cm depth from the top of the moss layer) varied significantly on a daily basis; the maximum daily mean temperature in the upper layer (0−15 cm) was observed in July in both 2014 and 2015.

The soil temperature in the deep layer increased slowly as the active layer thawed (Fig. 4b), indicating the seasonal variation across the full soil profile (5−60 cm). Above 30 cm depth, soil saturation was variable and not fully saturated at times, while the soil was always fully saturated below 30 cm depth. The water saturated soil of the upper (0−15 cm) and deeper soil layers (15−60 cm) had a volumetric water content of 80% and 60%, respectively. As the active layer thawed, soil ice turned into liquid water and the soil water content steadily increased to the layer's saturation point (Fig. 4c). The maximum thawing depth occurred in late September each year and reached 60 cm−80 cm deep, with a thawing speed of approximately 0.46 cm d^{-1} (Fig. 4d).

The dominant and secondary wind direction was northeast and southwest, respectively (Fig. 5a). Most of the wind from the east-northeast direction was at a low speed (<1.5 m s^{-1}) and occurred at nighttime. As a result, after strictly filtering, most of the accepted half-hourly fluxes occurred when winds were from west-southwest, with speeds of 1.5−3.5 m s^{-1} (Fig. 5b). Less wind came from the southeast and northwest directions, meaning that fewer strictly filtered half-hourly flux value were obtained under these wind directions.

3.2. Daily variations of methane emission

Strictly filtered fluxes were screened to reveal daily variations. Due to insufficient turbulence exchanges, most nighttime and early daytime methane fluxes could not pass the strict filtering. Consequently, the remaining values did not represent the actual diurnal variation patterns of the CH$_4$ emissions, because most available values (Fig. 6) were collected in the daytime (6:00 a.m. to 18:00).

Taking the poor quality of the nighttime data in period I of 2014 into consideration, the CH$_4$ emissions ranged from 0.13 to 0.44 mg m^{-2} h^{-1} with two CH$_4$ emission peaks, one occurring around 10:00 a.m. and another one around 14:00 p.m. (Fig. 6a). In period II of 2014, methane emissions stayed high (above 1.5 mg m^{-2} h^{-1}) between 9:00 a.m. and 15:00 p.m. with one emission peak (2.16 mg m^{-2} h^{-1}) at 12:30 (Fig. 6b). In period I of 2015, a few negative CH$_4$ fluxes were observed and the flux magnitude ranged from −0.05 to 0.14 mg m^{-2} h^{-1}; no diurnal peak was observed in this period (Fig. 6c). In period II of 2015, only one emission peak of 0.56 mg m^{-2} h^{-1} occurred at 9:30 a.m. (Fig. 6d). Daytime variability was observed in period II of both growing seasons. In period II of 2015, although the overall mean fluxes displayed diurnal variation clearly, the flux points of a single day (09/08/2015 as an example) could be of wide swings (Fig. 7a). Due to the relatively high emission rate in the same period of 2014, the
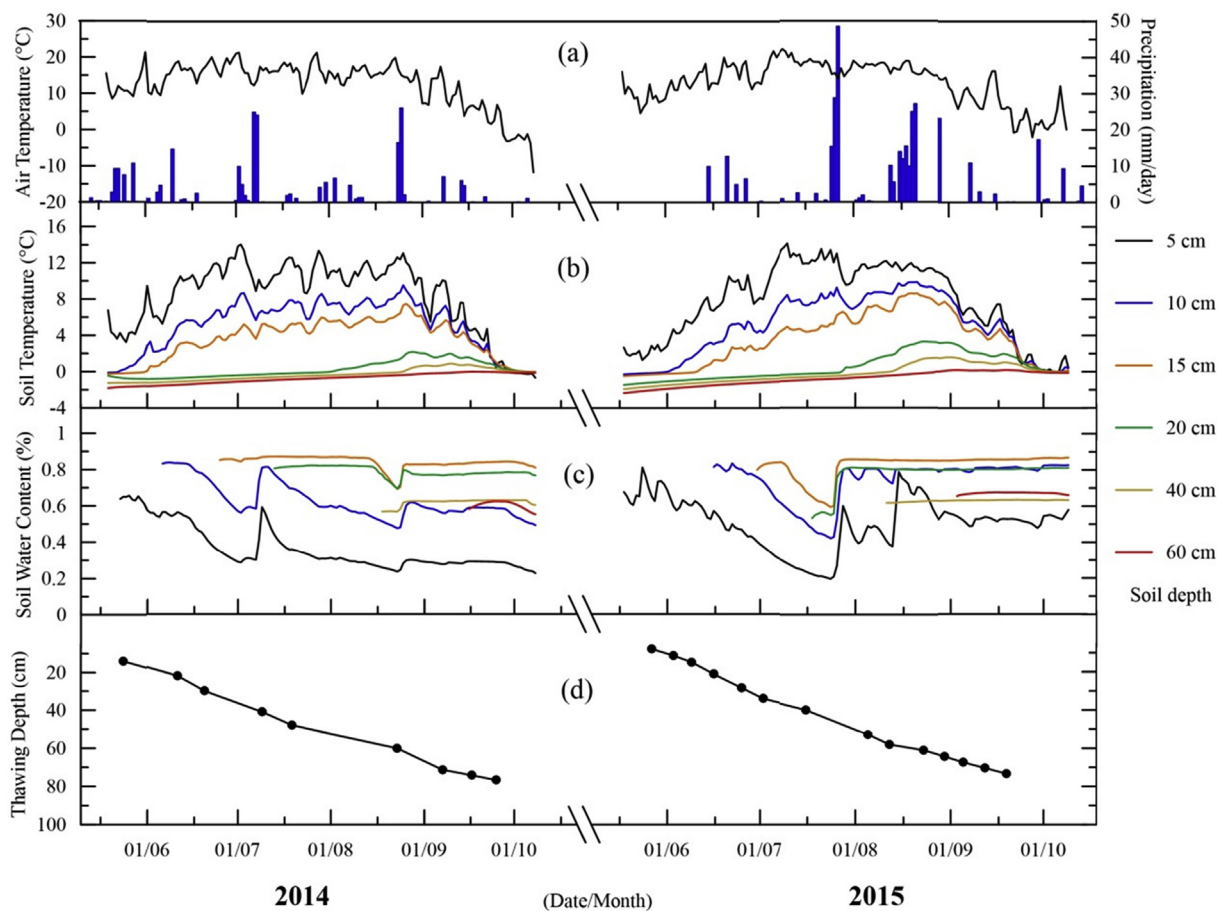
Fig. 4. Environmental conditions during the growing seasons. (a) Daily mean air temperature and daily precipitation; (b) daily mean soil temperature at different soil depths; (c) daily mean soil volume water content at different soil depths; (d) measured thawing depth marked as solid points.
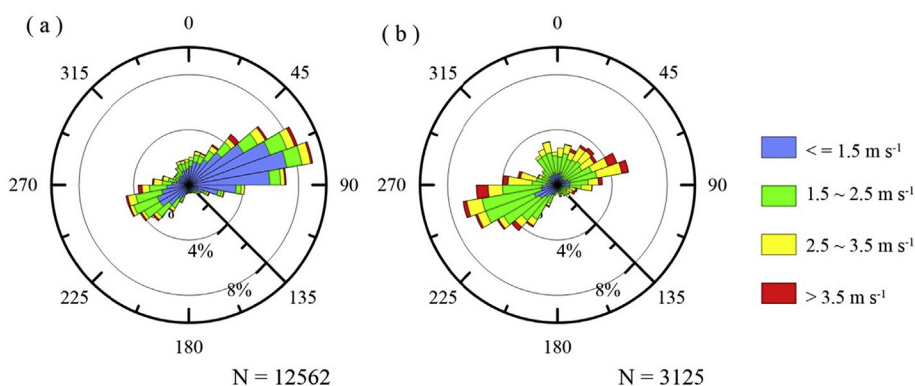

Fig. 5. (a) Half-hourly wind speed (m s^{-1}) and direction distribution of all data segments; (b) filtered data segments for analyses and regressions.

diurnal variation in one specific day (04/08/2015 as an example) was more clear (Fig. 7b). When wind direction kept stable (07/08/2015 as an example), a diurnal cycle was observed although fluxes were quite small (Fig. 7c). When the wind direction changed significantly from southwest to northeast at noon on 25/08/2015, the methane flux decreased at the same time which resulted in a more ambiguous diurnal cycle (Fig. 7d).

Eddy covariance observations from peatlands also showed significant diurnal methane emission cycles (Hommeltenberg et al., 2014; Long et al., 2009; Song et al., 2015). In these studies, a daily methane flux cycle was more apparent in the mid-summer and less apparent at the beginning and at the end of a growing season. Results from our study differed, in that apparent diurnal cycle occurred in August and September, after mid-summer. Other studies found no daily variations during any period (Iwata et al., 2015; Nadeau et al., 2013; Rinne et al., 2007).

In summary, when methane fluxes were large enough, diurnal emission patterns were easily detected. Conversely, when methane fluxes were relatively low, with high uncertainty, the changing microclimate conditions and high spatial variation masked daily
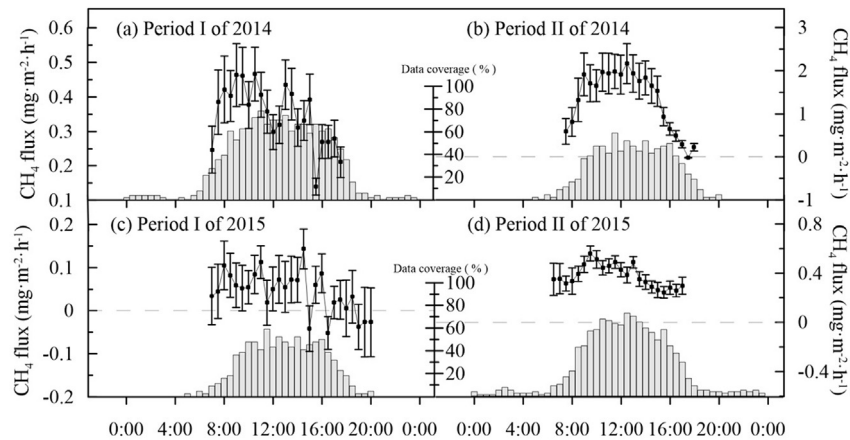
Fig. 6. Diurnal variation pattern of methane fluxes. Error bars represent the standard error of the mean. Bars indicate the percentage of available half-hourly fluxes in each period; total days were counted when at least one half-hourly data segment was available. The number of total days in (a) period I of 2014, (b) period II of 2014, (c) period I of 2015 and (d) period II of 2015 was 51, 44, 67 and 74 days, respectively.
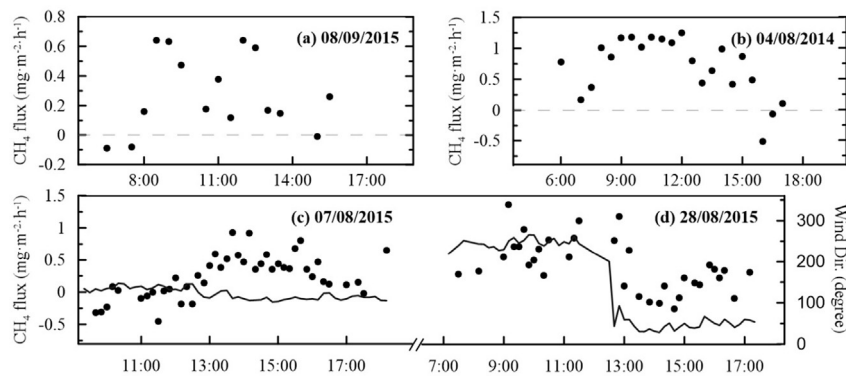
Fig. 7. Diurnal variation pattern of methane fluxes for specific days. (a) 08/09/2014 and (b) 04/08/2014 serve as examples in a single day of period II. A 10-min averaging period was selected as the averaging period to show more detailed variations within one day in (c) 07/08/2015 and (d) 28/08/2015. The black line in the two graphs represents wind direction (clockwise degrees separated from the north).

emission patterns in the northern peatland ecosystem, even assuming such a daily cycle existed (Hommeltenberg et al., 2014; Kowalska et al., 2013). Strictly filtering the calculated half-hour fluxes was very important when methane fluxes were relatively low.

3.3. Seasonal and spatial variability of methane flux

In 2014, the median values of the strictly filtered CH_4 fluxes in June, July, August, and September were 0.31, 0.34, 1.50 and 1.76 mg m^{-2} h^{-1}, respectively. The CH_4 fluxes in June and July were much lower than those in August and September. More than 75% of the fluxes were above zero (Fig. 8a). Methane flux in May and June of 2015 was negligible. The average flux of May did not significantly differ from zero (p = 0.91, not shown in plot), and the median flux of each month from May to October was −0.01, 0.05, 0.15, 0.33, 0.50 and 0.36 mg m^{-2} h^{-1}, respectively (Fig. 8b). Relatively large methane emission rates were found in period II of both 2014 and 2015, with concurrently broad inter-annual variations. Daily methane emissions showed the same trend (Fig. 8c and d).

The dominant wind directions in our study area were northeast and southwest (Fig. 5a). As a result, more data points of these directional sectors were included in the analysis. Within the wind direction of −60° (300°) ~ 60°, CH_4 fluxes were relatively low (p < 0.01), however, CH_4 fluxes in the wind direction of 90°−210°

were relatively high during period II of both years (Fig. 9). Low emissions, even negative fluxes, were observed in period I of 2015. Inversely, the flux in dominant wind direction was significantly large during the same period.

The spatial variation of the methane emissions can be explained by the local topography, which caused differences in hydrology regime and vegetation type. The terrain around the flux tower sloped from the northeast towards the southwest (Fig. 1c). Consequently, conditions were dryer to the northeast and wetter to the southwest. Because the fluxes with wind from the northwest and southeast were in low frequency range, dry and wet sectors were defined as 330° (−30°) ~ 90° and 150°−270°, respectively. The methane flux from the wet sector, to the southwest of the tower, was significantly higher than that from the dry sector (Fig. 10). This is consistent with results of other studies (Iwata et al., 2015; Olefeldt et al., 2013).

### 3.4. Methane emissions and environmental conditions

3.4.1. Water table level

As water table was not recorded during this study, a previous study was used as a reference. Miao et al. (2012) recorded seasonal changes of water table depth during the growing season of 2011 and 2012 within this study site. Water table dropped in the first half of growing season and then rose in the second half, with the lowest
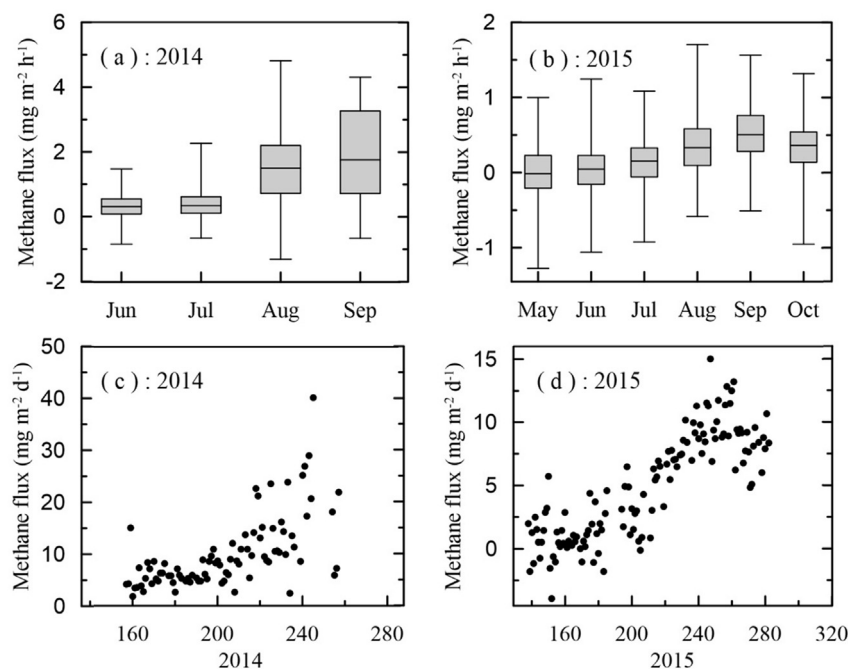
Fig. 8. Seasonal variations in methane flux. The box is defined by the lower and upper quartiles, and the line in the center of the box is the median. Whiskers show the minimum and maximum values. Points reflect calculated daily methane emissions. The x-axis of (c) and (d) represent Julian day of each growing season.
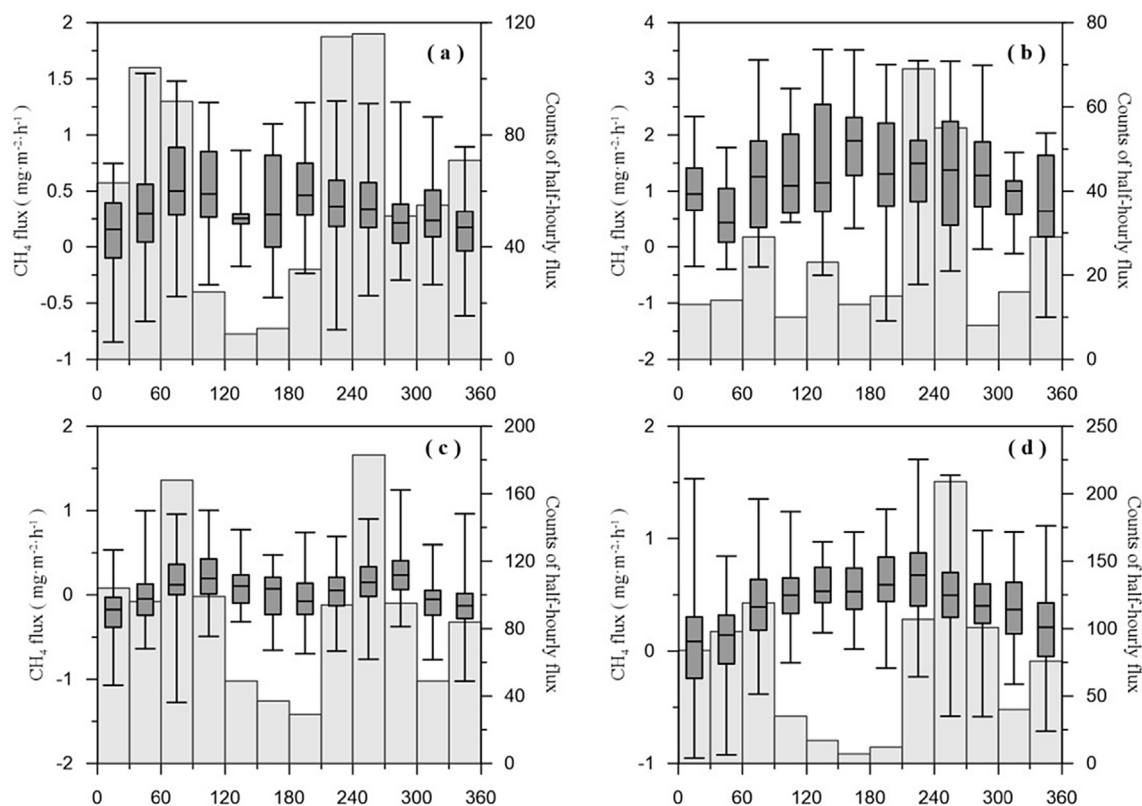
Fig. 9. Distribution of half-hourly CH_4 fluxes, according to wind direction (x axes), labels on x axis indicate degrees from north. Whiskers show the minimum and maximum values. The box is defined by the lower and upper quartiles, and the line in the center of the box is the median. Bar charts represent the number of half-hourly flux values in each period: (a) Period I of 2014, (b) period II of 2014, (c) period I of 2015 and (d) period II of 2015.

level appearing in July. Based on soil water content at different soil depths (Fig. 4c), the water content at 40 cm depth remained

constant, and water content at 20 cm depth was saturated across almost the entire growing season. This indicates that the water
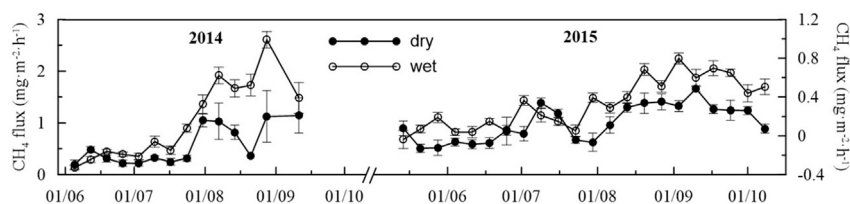
Fig. 10. Averaged (+/− s. e.) methane fluxes from the dry and wet sectors around the eddy covariance tower with an averaging time of seven days. The date format is dd/mm on the x axis.

table fluctuated between 0 and 20 cm below the ground surface, except for a short period in August. We didn't find any relationship between the water table and CH_4 flux which was similar with Hargreaves and Fowler (1998). When water table was relatively high (e. g. in June and September), methane emission was either high (in September) or low (in June).

Factors other than water table, such as plant phenology, soil temperature and solar radiation were changing simultaneously. Therefore, the regression between water table depth and methane flux did less help to determine the influence of water table. Water table is merely a factor that determined anaerobic volume, our study agrees with others in concluding that a relatively high water table level is an essential requirement to create anaerobic conditions for methanogens (Bubier et al., 1998; Hargreaves and Fowler, 1998; Rinne et al., 2007).

3.4.2. Thawing depth

The thawing depth consistently increased as the growing season progressed and it determined the lower boundary of the anaerobic conditions because of the existing continuous underlying permafrost. Seasonal thawing of the active layer is believed as a key regulator of CH_4 exchange in boreal peatlands (Iwata et al., 2015; Olefeldt et al., 2013) and arctic tundra (Kim, 2015). Due to variations in vegetative cover, the thawing depth was not the same across our study area. However, there was a significant correlation ($R^2 = 0.72$, $p < 0.01$ in 2014 and $R^2 = 0.75$, $p < 0.01$ in 2015) between the linearly interpolated thawing depth and the daily mean strictly filtered methane fluxes. The increasing depth of activity layer expanded the anaerobic volume. Meanwhile, the peat temperature in the deep layer (deeper than 15 cm) increased as thawing occurred. Both of these factors can enhance the methanogenic activity and could explain the higher CH_4 fluxes in the growing season (Fig. 8).

3.4.3. Peat temperature

Peat temperature below 20 cm depth correlated best with the daily mean strictly filtered methane flux (Table 1). This finding was consistent with Rinne et al. (2007), who found that peat temperature at a depth of 35 cm was the most highly correlated of all environmental factors with the daily average methane flux. Peat temperature below 20 cm depth is determined by seasonal thawing of the active layer and water exchange across the whole growing

season. The continuous moss layer in most northern peatlands provides a buffering effect, with low thermal conductivity, and could isolate the air and soil.

Our study's deep layer temperatures (e g. highest temperature of 3.3 °C at 20 cm depth in 2015) were very similar to those found at sites in Siberia and Alaska (Iwata et al., 2015; Nakano et al., 2000). According to Rinne et al. (2007), in Southern Finland (61° 50′ N), the highest temperature at 35 cm depth was approximately 15 °C. The presence of permafrost effectively reduced deep layer (>15 cm) temperatures. Even during late summer, when peat temperatures of all profiles were at their highest, they remained far below the optimum temperature for methanogens (25 °C).

An exponential equation form has been widely applied to explain the fundamental dependence of soil microbiological activity on temperature (Conrad et al., 1989; Kim et al., 1999). As methane production is a series of microbial activities, the relation between peat temperature and methane flux (Table 1) is likely to be exponential (Fig. 11). However, methane flux slowed down in late summer even though temperature was still increasing. This indicates that the deep layer peat temperature was not the only constraint on methane fluxes.

3.4.4. Vegetation

Within our study site, the vegetation community was dominated by shrub-mosses and *Eriophorum*. One plant manipulation experiment found that clipping the *Eriophorum* could reduce methane emissions by more than 70% (Miao et al., 2012). An in-situ moss removal experiment had less impact on CH_4 flux at our study site (Meng et al., 2014), although a similar experiment demonstrated a significant amount of methane oxidation at another Canadian peatland (Basiliko et al., 2004). In our study site, the vegetation distribution has not been plotted. Although we assumed that topography related vegetation difference might explain the spatial variability of methane emission, we did not find any solid evidence.

Vegetation is an important factor influencing peatland methane emissions (Lai, 2009). Plant root exudates and fine litter are easily decomposed by fermentation microbes, forming the methanogenesis substrate (Conrad, 1999; Large et al., 2009). Vascular plants with aerenchyma can transport methane; this occurs because of pressure gradients in different plant parts (Brix et al., 1996; Joabsson et al., 1999). Plant mediated transport is known as a dominant pathway in northern peatlands (Christensen, 1993; Frenzel and Rudolph, 1998; Sorrell and Boon, 1994). Nisbet et al. (2009) found that methane dissolved in soil pore water could also be emitted via plant evapotranspiration, regardless of whether there were aerenchyma tissues. This is consistent with Long et al. (2009), who found the diurnal pattern of CH_4 flux was strongly positively correlated with latent heat flux.

If vegetation significantly influenced CH_4 emissions at our site as above, then diurnal variation of CH_4 flux should be more apparent because plant activities are closely connected to rapidly changing factors such as photosynthetically available radiation (*PAR*), air

Table 1
Correlation coefficients of linear regression analysis comparing methane flux (based on natural logarithm) and environmental factors.

		Ts_{20}	Ts_{40}	Ts_{60}
F_{CH_4}	2014	0.7782	0.7519	0.7408
	2015	0.5992	0.6368	0.6375

An offset of 0.35 mg m^{-2} h^{-1} was added to the 2015 methane flux to ensure that the values were positive before logarithmic transformation. Ts_{20}, Ts_{40} and Ts_{60} correspond with soil temperature at 20, 40 and 60 cm depth. Statistical significance was below a P-value of 0.01.
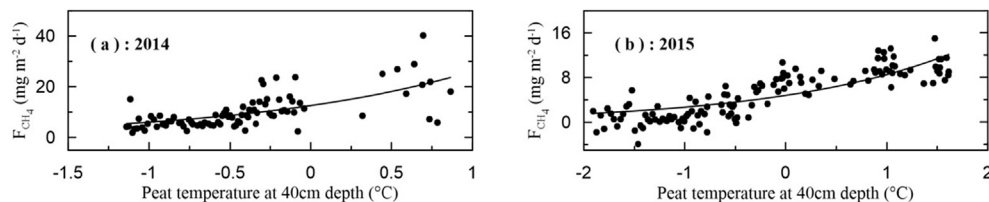
Fig. 11. Regression between daily methane flux and 40 cm deep peat temperature in two separate years. The fitted lines were determined using non-linear, least-square regressions.

temperature (T_a), atmospheric pressure (P), soil heat flux (H_s), vapor pressure (P_{vp}) and rainfall events. Instead, we found that the influence of vegetation on CH_4 flux was not important. This may also be the result of the low methane emissions as discussed in Section 3.3.

3.4.5. Model validation

A model based on Q_{10} theory (Equation (1) of Table 2) is often applied to interpret the dependence of methane emissions on water table and temperature (Bubier and Moore, 1994; Suyker et al., 1996). Another model (Equation (2) of Table 2) proposes that methane production and emissions are microbiologically induced processes, with temperature having an exponential impact (Rinne et al., 2007; Song et al., 2009, 2015). However, neither of the models considers seasonal thawing and freezing processes. These processes significantly influence soil thermal and hydrological conditions. Therefore, we tried to take them into account and modify the commonly used statistical models for peat CH_4 production.

Parameters with regular seasonal variations, such as root distribution and lower boundary temperatures of modeled soil profiles, have been interpreted as a function of the Julian day in some process-based models (Jansson and Karlberg, 2010; Zhang et al., 2002). We parameterized seasonal thawing and freezing similarly: as a combination of a term based on a nonstandard Gaussian curve and a term based on a logistic curve (Equation (3) of Table 2). According to Miao et al. (2012) and our observations, thawing generally begins in early May; the maximum thawing depth occurs around September 20th. Soon thereafter, the peat begins to freeze and the upper layer (<15 cm) of the soil completely freezes within 20 days. Considering equation (3), the thawing depth can be normalized and represented as a function of Julian day, and then visualized (Fig. 12) with localized parameters (Table 2).

Although there was variability within a relatively small range, the deep layer temperatures were strongly correlated with thawing depth. This could indicate concurrent microbial activity (methane

production). Therefore, the 40 cm peat temperature (T_{40}) was selected as the indicator, and the exponential regression equation (Equation (4) of Table 2) was applied to assess the influence of peat temperature on methane emissions (Fig. 11). Table 3 displays the parameters and performance of equation (4). With the relatively low regression quality ($R^2 = 0.43$ in 2014 and $R^2 = 0.67$ in 2015), this equation is inadequate to predict methane emission patterns. By taking the seasonal thawing into account, equation (4) was modified to equation (5) (Table 2). Table 3 and Fig. 13 show the
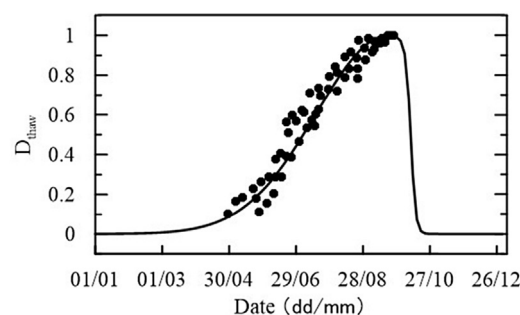

Fig. 12. Visualization of thawing depth term during the growing season. The points indicate normalized field observations of the thawing depth in this study and Miao et al. (2012).

Table 3
Parameters and performance of equations (4) and (5) when interpreting the correlation between daily methane emissions and 40 cm depth peat temperature.

	Year	a	b	R^2	SSE
Equation (4)	2014	12.559	0.731	0.431	2346.2
	2015	4.797	0.575	0.666	720.7
Equation (5)	2014	16.220	0.320	0.449	2270.0
	2014M	15.110	0.318	0.725	363.4
	2015	6.984	0.303	0.765	507.5

SSE represents sum of squared errors.

Table 2
List of equations.

Equation	No.	Definition
$F = a \cdot 10^{bW} \cdot c^{\frac{T-T_{ref}}{10}}$	(1)	a, b and c: parameters
$F = a \cdot e^{bT} + c$	(2)	F: methane emission rate;
		W: water table; T: temperature;
		T_{ref}: reference temperature
$D_{thaw} = e^{\frac{-(D-D_{max})^2}{0.5 \times L_{th}^2}} \times \frac{e^{-c \times (D-D_{mf})}}{1+e^{-c \times (D-D_{mf})}}$	(3)	a, b: parameters;
		c: freezing speed constant (0.4595)
$F^*_{CH_4} = a \times e^{b \times T_{40}}$	(4)	$F^*_{CH_4}$ and: F_{CH_4}: methane flux
$F_{CH_4} = a \times D_{thaw} \times e^{b \times T_{40}}$	(5)	D_{thaw}: thawing item;
		D: Julian day
		D_{max}: Julian day of maximum thawing depth (day 263 as a constant)
		L_{th}: duration of thawing process (130 days as a constant)
		D_{mf}: Julian day when peat was half-frozen (day 283 as a constant)

Parameter a represents methane emission potential, parameter b represents sensitivity of water table (in equation (1)) or temperature (in equations (2), (4) and (5)), parameter c determines the minimum value of methane flux.
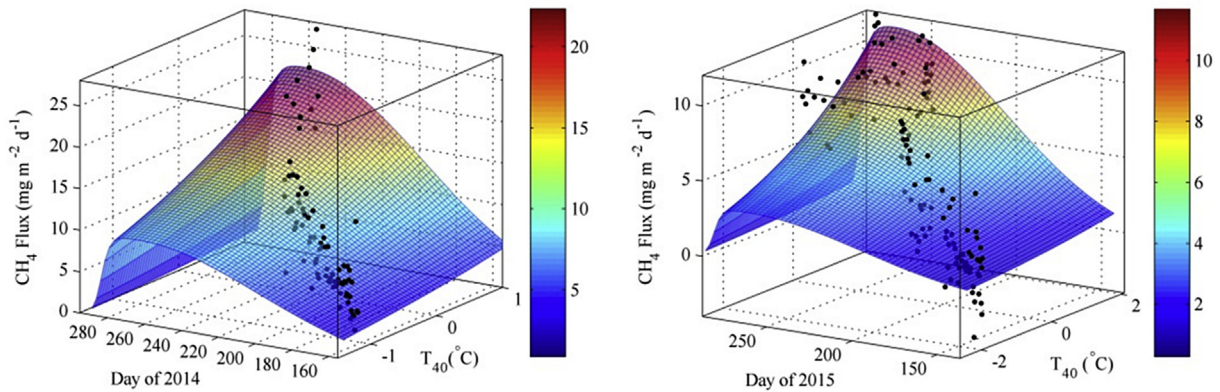
Fig. 13. Influence of 40 cm deep peat temperature and permafrost thawing on methane emission in two separated years. The X axis represents Julian day of a year; the Y axis represents temperature at the depth of 40 cm; the Z axis represents daily methane emissions. One extreme point with high daily methane emission (40.2 mg m^{-2} d^{-1}) in 2014 was omitted.

regression between the daily CH_4 fluxes and the peat temperature at the depth of 40 cm. Equation (5) was statistically more precise than equation (4) in both years. The difference between the observed and the predicted daily emission was defined as residual, positive values meant that observed daily emissions were higher than predicted daily emissions. Most residuals (>90%) during 2015 were within ±5 mg m^{-2} d^{-1} while several points with relatively large residuals (>10 mg m^{-2} d^{-1}) existed in period II of 2014 (Fig. 14).

To examine the influence of these large residuals on the regression, we performed the regression again after removing these outliers with residuals >5 mg m^{-2} d^{-1}. The results (2014M in Table 3) demonstrated that those positive residuals could overestimate methane emission potential (Parameter a) by 7.3%. The outliers did not show much influence on temperature sensitivity (Parameter b in Equation (5)). However, this evaluation was based on our existing data. Data in September and October were limited because of system malfunctions, which could add more uncertainty. The temperature sensitivity of the two growing seasons were similar and were comparable with Rinne et al. (2007), who found that temperature sensitivity at a depth of 35 cm was approximately 0.25 °C^{-1}.

Statistically, the residuals should vary randomly and 5-day moving average of the residuals is shown in Fig. 14. We found that heavy rain events coincided with times when the residuals began to increase. After increasing for several days, the residuals tended to decrease again (including sunny, cloudy and drizzly days). The curve will not align with the variation of water table depth because the water table would rise immediately after heavy rain events (Table 4). This lag could be explained by Brown et al. (2014) who reported a hysteresis between the water table and the CH_4 flux. This agreement indicates that soil hydrological

Table 4
The rain events displayed in Fig. 14.

Year	No.	Date (dd/mm)	Julian day	Precipitation (mm)
2014	1	7/7−8/7	188−189	49.2
	2	29/7	210	21.4
		31/7	211	
		3/8	216	
		8/8	220	
	3	24/8−25/8	236−237	42.8
2015	4	21/6	172	12.8
	5	25/7−27/7	206−208	92.8
	6	29/8	241	23.3
	7	8/9	251	11
	8	30/9	273	17.4

condition also contributed to methane emissions. Therefore, a relatively low water table depth or a long period with no precipitation could restrict methane emission in mid-summer. As this hysteresis was observed in the plot of residuals, the water table variation had influenced methane flux in a small magnitude at our study site. The lack of water table measurements made it difficult for us to quantify this influence.

3.5. Growing season methane emission budget

An estimated 1.52 g m^{-2} was emitted in the growing season of 2014 (143 days from May 19th to October 8th); a smaller amount of 0.71 g m^{-2} was emitted in the growing season of 2015 (145 days from May 18th to October 9th). These results were almost the same (1.46 g m^{-2} and 0.71 g m^{-2} in 2014 and 2015, respectively) when all daily fluxes including the observed ones were predicted by the obtained equation (5). Compared to field observations in other
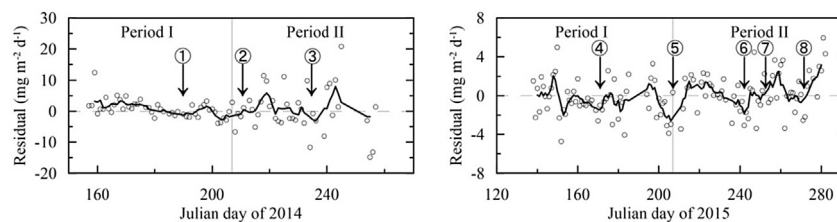
Fig. 14. Residuals distribution of the regression equation (5) along with Julian days in two growing seasons. Residuals were calculated as the difference between the observed and the estimated value (a positive residual indicated that the observed daily methane emission was higher than the estimated value). The solid line represented the moving average of the residuals in a window of 5 days. Number 1−8 indicated the time when heavy rain events occurred (Table 4).

northern peatlands, CH_4 flux at our site was significantly lower by almost an order of magnitude (Table 5).

Our results were consistent with other studies of permafrost peatlands (Iwata et al., 2015) and Siberian tundra (Christensen, 1993) at higher latitudes. Unlike European sites, which have oceanic climate types with warmer and wetter winters, the typical continental climate of the Great Hing'an Mountains creates dryer and colder winters at the same latitude. The wide spread moss also helps to reduce the summer peat temperature. This, in turn, keeps methane production low. Moreover, the study site is poor in soil nutrients (most carbon and nitrogen is in an organic form) and the water supply of the peatland is limited; these conditions further constrain methanogenic activity. Taken together, these conditions make the permafrost peatland in the Great Hing'an Mountains a weak source of methane. However, the area has the potential for significant methane emissions because of its large carbon storage capacity and vulnerability to climate change.

3.6. The inter-annual variation of growing season methane emission

The inter-annual variation in CH_4 emission is seldom discussed in literature. Some reports have found that high methane emissions occurred in relatively warmer and wetter years (Iwata et al., 2015; Olson et al., 2013; Tagesson et al., 2012). However, the results of our study do not completely agree with these studies.

Growing season methane flux at the same site from 2010 to 2015 (including our eddy covariance observation) were summarized to explain the abnormal inter-annual variations (Table 6). We used flux ranges instead of absolute budget, because the static chambers used by previous researches (Meng et al., 2014; Miao et al., 2012) were only conducted in the area covered by shrub and moss. In the growing season of 2013, when precipitation was almost double the multi-year average, methane emissions were substantially higher. During the growing season of 2014, there was only 236.9 mm of rainfall, but methane emissions were considerably higher than in 2015 both in terms of the maximum daily flux in late summer and the overall average flux across the whole growing season.

A hypothesis based on previous in-situ methane emissions is that seasonal permafrost thawing and freezing may play an important role in controlling methane emissions. At the end of a growing season, the top layer of the soil typically freezes before the deep layer. This isolates the soil from the atmosphere. CH_4 may be generated in the subsurface but not be released. We have observed high pore-water CH_4 concentrations late in the growing season (unpublished data). Further, a burst of CH_4 from the permafrost shortly after thawing is frequently observed. In such cases, most of the released methane was present before thawing instead of originating during the thawing process (Rachel et al., 2011). Due to permafrost, the soil then gradually thaws from the top layer to the deep layer and the thawing process lasts during a whole growing season. The existing methane stored in one specific layer will not be released until the corresponding layer thawed.

The inter-annual variation of our site may be used as an example. The precipitation of the growing season in 2013 was substantially larger than the multi-year average, which led to significantly higher methane production and emission. Under these conditions, it is likely that abundant CH_4 was sealed in the frozen active layer during late in the growing season of 2013. The abundant CH_4 was gradually released during the thawing process in the following year. Similarly, low methane production in 2014 because of the drought could result in low methane emissions in 2015.

Growing season precipitation influences soil thermal and hydrological conditions, determining for example water table depth, peat temperature and maximum thawing depth. More heat is carried to the deeper layers by infiltration than by thermal conduction due to the low thermal conductance of the peat and the high efficiency of water infiltration. The heat carried to the deep layer significantly increases the temperature, and also promotes the thawing of the bottom permafrost. This condition can stimulate methane production processes, and contribute to a higher emission rate. Without permafrost, however, the whole soil profile would melt in the spring and the trapped methane could be released rapidly within several days. This could explain the spring pulse of CH_4 emissions in some temperate and boreal wetlands that do not have underlying permafrost (Song et al., 2012).

With simple environmental parameters such as air temperature and precipitation, process-based geochemistry wetland models and multiyear regressions can be used to simulate deep layer temperatures. However, with existing data, it is difficult to evaluate the inter-annual variability and predict the CH_4 emission potential for a specific year. The relationship between methane emission potential and growing season precipitation is also difficult to figure out. Therefore, further observations of CH_4 emissions and carefully planned experiments such as isotope labeling and intact frozen peat core melting experiments were needed to validate our hypothesis.

4. Conclusions

This study focused on interpreting methane emission patterns and their controlling factors in a permafrost peatland of the Great Hing'an Mountains, Northeast China. The open-path eddy covariance method and meteorological observations were made during

Table 5
Reviews of methane emission budgets in several northern wetlands (sorted by latitude).

Measuring method	Methane budget (g CH_4 m^{-2})	Period	Location	Latitude	Wetland type	Reference
Eddy covariance	0.71—1.52	May to October	The Great Hing'an Mountains, China	52°56′N	Oligotrophic bog	This study
Static chamber	1.633	May to October	Central Canada	45°04′N	Swamp	Roulet et al. (1992)
Static chamber	20—39	June to October	Minnesota, the U.S.	47°32′N	Forested peat bog and fen	Dise (1993)
Static chamber	9.3—21.4	June to September	Minnesota, the U.S.	48°N	Bog and fen	Chasar et al. (2000)
Static chamber	3.3—13.0	One year	Glencar, Ireland	51°55′N	Blanket bog	Laine et al. (2007)
Eddy covariance	4.4	June to September	Northern Quebec, Canada	53°40′N	Bog	Nadeau et al. (2013)
Eddy covariance	12.6	One year	Southern Finland	61°50′N	Oligotrophic fen	Rinne et al. (2007)
Eddy covariance	4.98	April to September	Alaska, the U.S.	64°42′N	Permafrost peat bog	Euskirchen et al. (2014)
Eddy covariance	0.48—0.72	May to October	Alaska, the U.S.	64°52′N	Permafrost peat bog	Iwata et al. (2015)
Eddy covariance	24.5—29.5	One year	Northern Sweden	68°20′N	Mire	Marcin et al. (2010)
Automatic chamber	0.17—12.1	June to September	Northern Sweden	68°22′N	Mire	Bäckstrand et al. (2008)
Static chamber	0.067—8.83	One year	Alaska, the U.S.	68°38′N	Tundra	Christensen (1993)
Gradient method	2.40—6.18	June to August	Alaska, the U.S.	69°10′N	Tundra	Harazono et al. (2006)
Eddy covariance	3.15	One year	Lena River Delta, Russia	72°22′N	Tundra	Wille et al. (2008)
Eddy covariance	5.0—7.1	May to October	Zackenberg, Greenland	74°28′N	Fen	Tagesson et al. (2012)

Table 6
The range of daily methane emissions of the growing seasons and the corresponding total precipitation of the study site during 2010–2015.

Year	2010	2011	2012	2013	2014	2015
Precipitation in growing season(mm)	325.9	496.2	347.1	621.4	236.9	333
Measuring method	Static chamber				Eddy Covariance	
Daily Methane emission (mg m^{-2} d^{-1})	−0.5–12.2	0.5–32.4	0.5–13.2	0.2–116.2	1.8–40.2	−3.9–15.0
Reference	Miao et al. (2012)		Meng et al. (2014)		This study	

the growing season of 2014 and 2015. Strict filtering criteria were used to screen calculated half-hourly fluxes, as more accurate data provide improved insights on the emission patterns. Microclimate data showed the influence of environmental factors on methane emissions.

The strictly filtered flux results demonstrated that methane emissions exhibited significant seasonal variation, with higher emissions present during the second half of growing seasons. Approximately 77.9% and 85.9% of total growing season emissions were released after July 25th of 2014 and 2015 respectively. More distinct diurnal variations and trends were seen after July 25th of each growing season. The daily methane exchange ranged from 1.8 to 40.2 mg m^{-2} d^{-1} in 2014 and from −3.9 to 15.0 mg m^{-2} d^{-1} in 2015. The total budget of the growing season of 2014 and 2015 was 1.52 g m^{-2} and 0.71 g m^{-2}, respectively.

In addition to temporal variability, methane emissions also exhibited spatial variability due to subtle differences in topography that created drier and wetter areas. Wetter sectors emitted more methane during most seven-day-average periods. Of all the measured environmental factors, only temperature in the deep layer (>15 cm) was significantly correlated with methane emissions. We modified and applied an empirical model based on an exponential temperature response to evaluate methane emissions at our study site. The model's performance was improved when a thawing term was added to the temperature response equation, confirming that the thawing process was a key factor as reported in previous studies.

Although permafrost peatlands in the Great Hing'an Mountains currently only emit small amounts of methane, emissions are expected to increase with higher temperature and more precipitation. Further observations and experiments are needed to improve our understanding of processes controlling methane production and emission, given the vital nature of carbon-climate feedback in the permafrost in the context of climate change.

Acknowledgements

References

Aubinet, M., Vesala, T., Papale, D., 2012. Eddy Covariance: a Practical Guide to Measurement and Data Analysis. Springer, pp. 365–376.

Aurela, M., Lohila, A., Riutta, T., Tuovinen, J.P., Hatakka, J., Laurila, T., 2009. Carbon dioxide exchange on a northern boreal fen. Boreal Environ. Res. 14, 699–710.

Bäckstrand, K., Crill, P.M., Mastepanov, M., Christensen, T.R., Bastviken, D., 2008. Total hydrocarbon flux dynamics at a subarctic mire in northern Sweden. J. Geophys. Res. Biogeosciences 113, 119–128.

Baldocchi, D., Detto, M., Sonnentag, O., Verfaillie, J., Teh, Y.A., Silver, W., Kelly, N.M., 2012. The challenges of measuring methane fluxes and concentrations over a peatland pasture. Agric. For. Meteorology 153, 177–187.

Baldocchi, D.D., 2003. Assessing the eddy covariance technique for evaluating carbon dioxide exchange rates of ecosystems: past, present and future. Glob. Change Biol. 9, 479–492.

Basiliko, N., Knowles, R., Moore, T.R., 2004. Roles of moss species and habitat in methane consumption potential in a northern peatland. Wetlands 24, 178–185.

Beetz, S., Liebersbach, H., Glatzel, S., Jurasinski, G., 2012. Effects of land use intensity on the full greenhouse gas balance in an Atlantic peat bog. Biogeosciences Discuss. 10, 1067–1082.

Bergman, I., Bo, H.S., Nilsson, M., 1998. Regulation of methane production in a Swedish acid mire by pH, temperature and substrate. Soil Biol. Biochem. 30, 729–741.

Brix, H., Sorrell, B.K., Schierup, H.-H., 1996. Gas fluxes achieved by in situ convective flow in Phragmites australis. Aquat. Bot. 54, 151–163.

Brown, M.G., Humphreys, E.R., Moore, T.R., Roulet, N.T., Lafleur, P.M., 2014. Evidence for a nonmonotonic relationship between ecosystem-scale peatland methane emissions and water table depth. J. Geophys. Res. Biogeosciences 119, 826–835.

Bubier, J.L., Crill, P.M., Moore, T.R., Savage, K., Varner, R.K., 1998. Seasonal patterns and controls on net ecosystem CO_2 exchange in a boreal peatland complex. Glob. Biogeochem. Cycles 12, 703–714.

Bubier, J.L., Moore, T.R., 1994. An ecological perspective on methane emissions from northern wetlands. Trends Ecol. Evol. 9, 460–464.

Chasar, L.S., Chanton, J.P., Glaser, P.H., Siegel, D.I., 2000. Methane concentration and stable isotope distribution as evidence of Rhizospheric processes: comparison of a fen and bog in the glacial lake agassiz peatland complex. Ann. Bot. 86, 655–663.

Christensen, T.R., 1993. Methane emission from Arctic tundra. Biogeochemistry 21, 117–139.

Christensen, T.R., Jonasson, S., Callaghan, T.V., Havström, M., 1995. Spatial variation in high-latitude Methane flux along A transect across Siberian and European tundra environments. J. Geophys. Res. Atmos. 1002, 21035–21046.

Conrad, R., 1999. Contribution of hydrogen to methane production and control of hydrogen concentrations in methanogenic soils and sediments. Fems Microbiol. Ecol. 28, 193–202.

Conrad, R., Andreae, M.O., Schimel, D.S., 1989. Control of methane production in terrestrial ecosystems. Exch. Trace Gases Between Terr. Ecosyst. Atmos. 808, 39–58.

Davidson, E., Savage, K., Verchot, L., Navarro, R., 2002. Minimizing artifacts and biases in chamber-based measurements of soil respiration. Agric. For. Meteorology 113, 21–37.

Dirk, W., André, L., Arndt, E., Andreas, G., 2005. Methane fluxes in permafrost habitats of the Lena Delta: effects of microbial community structure and organic matter quality. Environ. Microbiol. 7, 1582–1592.

Dise, N.B., 1993. Methane emission from Minnesota peatlands: spatial and seasonal variability. Glob. Biogeochem. Cycles 7, 123–142.

Euskirchen, E.S., Edgar, C.W., Turetsky, M.R., Waldrop, M.P., Harden, J.W., 2014. Differential response of carbon fluxes to climate in three peatland ecosystems that vary in the presence and stability of permafrost. J. Geophys. Res. Biogeosciences 119, 1576–1595.

Falge, E., Baldocchi, D., Olson, R., Anthoni, P., Aubinet, M., Bernhofer, C., Burba, G., Ceulemans, R., Clement, R., Han, D., 2001. Gap filling strategies for defensible annual sums of net ecosystem exchange. Agric. For. Meteorology 107, 43–69.

Foken, T., Göeckede, M., Mauder, M., Mahrt, L., Amiro, B., Munger, W., 2004. Post-field Data Quality Control. Springer, Netherlands.

Foken, T., Leuning, R., Oncley, S.R., Mauder, M., Aubinet, M., 2012. Corrections and Data Quality Control. Springer, Netherlands.

Frenzel, P., Rudolph, J., 1998. Methane emission from a wetland plant: the role of CH_4 oxidation in Eriophorum. Plant & Soil 202, 27–32.

Fung, I., John, J., Lerner, J., Matthews, E., Prather, M., Steele, L.P., Fraser, P.J., 1991. Three-dimensional model synthesis of the global methane cycle. J. Geophys. Res. Atmos. 96, 13033–13065.

Funk, D.W., Pullman, E.R., Peterson, K.M., Crill, P.M., Billings, W., 1994. Influence of water table on carbon dioxide, carbon monoxide, and methane fluxes from taiga bog microcosms. Glob. Biogeochem. Cycles 8, 271–278.

Gorham, E., 1991. Northern peatlands: role in the carbon cycle and probable responses to climatic warming. Ecol. Appl. 1, 182–195.

Gu, L., Falge, E.M., Boden, T., Baldocchi, D.D., Black, T.A., Saleska, S.R., Suni, T., Verma, S.B., Vesala, T., Wofsy, S.C., Xu, L., 2005. Objective threshold determination for nighttime eddy flux filtering. Agric. For. Meteorology 128, 179–197.

Hanis, K.L., Amiro, B.D., Tenuta, M., Papakyriakou, T., Swystun, K.A., 2015. Carbon exchange over four growing seasons for a subarctic sedge fen in northern Manitoba, Canada. Arct. Sci. 1, 27–44.

Harazono, Y., Mano, M., Miyata, A., Yoshimoto, M., Zulueta, R.C., Vourlitis, G.L., Kwon, H., Oechel, W.C., 2006. Temporal and spatial differences of methane flux at arctic tundra in Alaska. Memoirs Natl. Inst. Polar Res. Special Issue 59, 79–95.

Hargreaves, K.J., Fowler, D., 1998. Quantifying the effects of water table and soil temperature on the emission of methane from peat wetland at the field scale. Atmos. Environ. 32, 3275—3282.

Hinkel, K.M., Outcalt, S.I., 1994. Identification of heat-transfer processes during soil cooling, freezing, and thaw in central Alaska. Permafr. Periglac. Process. 5, 217—235.

Hommeltenberg, J., Mauder, M., Drösler, M., Heidbach, K., Werle, P., Schmid, H.P., 2014. Ecosystem scale methane fluxes in a natural temperate bog-pine forest in southern Germany. Agric. For. Meteorology 198—199, 273—284.

Hosono, T., Nouchi, I., 1997. The dependence of methane transport in rice plants on the root zone temperature. Plant Soil 191, 233—240.

Imelda, S., Baird, A.J., Heppell, C.M., 2013. The importance of ebullition as a mechanism of methane (CH_4) loss to the atmosphere in a northern peatland. Geophys. Res. Lett. 40, 2087—2090.

IPCC, 2013. Climate change 2013. In: The Physical Science Basis, Working Group I Contribution to the Fifth Assessment Report of the Intergovernmental Panel on Climate Change. Cambridge University Press, New York.

Iwata, H., Harazono, Y., Ueyama, M., Sakabe, A., Nagano, H., Kosugi, Y., Takahashi, K., Kim, Y., 2015. Methane exchange in a poorly-drained black spruce forest over permafrost observed using the eddy covariance technique. Agric. For. Meteorology 214—215, 157—168.

Jansson, P.-E., Karlberg, L., 2010 (Stockholm). In: Technology, R.I.o. (Ed.), Coupled Heat and Mass Trans-fer Model for Soil-plant-atmosphere Systems.

Joabsson, A., Christensen, T.R., Wallén, B., 1999. Vascular plant controls on methane emissions from northern peatforming wetlands. Trends Ecol. Evol. 14, 385—388.

Joosten, H., Clarke, D., 2002. Wise use of Mires and Peatlands. International mire conservation group.

Juszczak, R., 2013. Biases in methane chamber measurements in peatlands. Int. Agrophysics 27, 159—168.

Kim, J., Verma, S.B., Billesbach, D.P., 1999. Seasonal variation in methane emission from a temperate Phragmites-dominated marsh: effect of growth stage and plant-mediated transport. Glob. Change Biol. 5, 433—440.

Kim, Y., 2015. Effect of thaw depth on fluxes of CO_2 and CH_4 in manipulated Arctic coastal tundra of Barrow, Alaska. Sci. Total Environ. 505, 385—389.

Kljun, N., Calanca, P., Rotach, M.W., Schmid, H.P., 2004. A simple parameterisation for flux footprint predictions. Boundary-Layer Meteorol. 112, 503—523.

Kokelj, S.V., Tunnicliffe, J., Lacelle, D., Lantz, T.C., Chin, K.S., Fraser, R., 2015. Increased precipitation drives mega slump development and destabilization of ice-rich permafrost terrain, northwestern Canada. Glob. Planet. Change 129, 56—68.

Kowalska, N., Chojnicki, B.H., Rinne, J., Haapanala, S., Siedlecki, P., Urbaniak, M., Juszczak, R., Olejnik, J., 2013. Measurements of methane emission from a temperate wetland by the eddy covariance method. Int. Agrophysics 27, 283—290.

Laetitia, I., Adrian, S., Renato, S., Valérie, M.D., Thomas, B., Bénédicte, L., Jean-Marc, B., Dominique, R., Stocker, T.F., Chappellaz, J., 2008. Orbital and millennial-scale features of atmospheric CH_4 over the past 800,000 years. Nature 453, 383—386.

Lai, C.T., Katul, G., Butnor, J., Ellsworth, D., Oren, R., 2002. Modelling night-time ecosystem respiration by a constrained source optimization method. Glob. Change Biol. 8, 124—141.

Lai, D.Y.F., 2009. Methane dynamics in northern peatlands: a review. Pedosphere 19, 409—421.

Laine, A., Wilson, D., Kiely, G., Byrne, K.A., 2007. Methane flux dynamics in an Irish lowland blanket bog. Plant & Soil 299, 181—193.

Large, D.J., Spiro, B., Ferrat, M., Shopland, M., Kylander, M., Gallagher, K., Li, X., Shen, C., Possnert, G., Zhang, G., 2009. The influence of climate, hydrology and permafrost on Holocene peat accumulation at 3500 m on the eastern Qing-hai—Tibetan Plateau. Quat. Sci. Rev. 28, 3303—3314.

Long, K.D., Flanagan, L.B., Cai, T., 2009. Diurnal and seasonal variation in methane emission in a northern Canadian peatland measured by eddy covariance. Glob. Change Biol. 16, 2420—2435.

Marcin, J.K., Christensen, T.R., Kristina, B., Patrick, C., Thomas, F., Mikhail, M., Lena, S., 2010. Annual cycle of methane emission from a subarctic peatland. J. Geophys. Res. Biogeosciences 115, 590.

Mcveigh, P., Sottocornola, M., Foley, N., Leahy, P., Kiely, G., 2014. Meteorological and functional response partitioning to explain interannual variability of CO_2 exchange at an Irish Atlantic blanket bog. Agric. For. Meteorology 194, 8—19.

Meng, H.N., Song, C.C., Miao, Y.Q., Mao, R., Wang, X.W., 2014. Response of CH_4 emission to moss removal and N addition in boreal peatland of Northeast China. Biogeosciences 11, 3365—3385.

Metje, M., Frenzel, P., 2007. Methanogenesis and methanogenic pathways in a peat from subarctic permafrost. Environ. Microbiol. 9, 954—964.

Miao, Y., Mao, R., Song, C., Sun, L., Wang, X., Meng, H., 2012. Growing season methane emission from a boreal peatland in the continuous permafrost zone of Northeast China: effects of active layer depth and vegetation. Biogeosciences Discuss. 9, 4455—4464.

Moncrieff, J., Clement, R., Finnigan, J., Meyers, T., 2004. Averaging, Detrending, and Filtering of Eddy Covariance Time Series. Springer Netherlands.

Moncrieff, J.B., Massheder, J.M., Bruin, H.D., Elbers, J., Friborg, T., Heusinkveld, B., Kabat, P., Scott, S., Soegaard, H., Verhoef, A., 1997. A system to measure surface fluxes of momentum, sensible heat, water vapour and carbon dioxide. J. Hydrology 189, 589—611.

Moore, C.J., 1986. Frequency response corrections for eddy correlation systems. Boundary-Layer Meteorol. 37, 17—35.

Moore, T., Dalva, M., 1993. The influence of temperature and water table position on carbon dioxide and methane emissions from laboratory columns of peatland soils. J. Soil Sci. 44, 651—664.

Moore, T., Knowles, R., 1989. The influence of water table levels on methane and carbon dioxide emissions from peatland soils. Can. J. Soil Sci. 69, 33—38.

Nadeau, D.F., Rousseau, A.N., Coursolle, C., Margolis, H.A., Parlange, M.B., 2013. Summer methane fluxes from a boreal bog in northern Quebec, Canada, using eddy covariance measurements. Atmos. Environ. 81, 464—474.

Nakai, T., Shimoyama, K., 2012. Ultrasonic anemometer angle of attack errors under turbulent conditions. Agric. For. Meteorology 162—163, 14—26.

Nakano, T., Kuniyoshi, S., Fukuda, M., 2000. Temporal variation in methane emission from tundra wetlands in a permafrost area, northeastern Siberia. Atmos. Environ. 34, 1205—1213.

Nisbet, R.E., Fisher, R., Nimmo, R.H., Bendall, D.S., Crill, P.M., Gallego-Sala, A.V., Hornibrook, E.R., López-Juez, E., Lowry, D., Nisbet, P.B., 2009. Emission of methane from plants. Proc. R. Soc. B Biol. Sci. 276, 1347—1354.

Nykänen, H., Heikkinen, J.E.P., Pirinen, L., Tiilikainen, K., Martikainen, P.J., 2003. Annual CO_2 exchange and CH_4 fluxes on a subarctic palsa mire during climatically different years. Glob. Biogeochem. Cycles 17, 1018.

Olefeldt, D., Turetsky, M.R., Crill, P.M., Mcguire, A.D., 2013. Environmental and physical controls on northern terrestrial methane emissions across permafrost zones. Glob. Change Biol. 19, 589—603.

Olson, D.M., Griffis, T.J., Noormets, A., Kolka, R., Chen, J., 2013. Interannual, seasonal, and retrospective analysis of the methane and carbon dioxide budgets of a temperate peatland. J. Geophys. Res. Biogeosciences 118, 226—238.

Rachel, M., Waldrop, M.P., Deangelis, K.M., David, M.M., Chavarria, K.L., Blazewicz, S.J., Rubin, E.M., Jansson, J.K., 2011. Metagenomic analysis of a permafrost microbial community reveals a rapid response to thaw. Nature 480, 368—371.

Ran, Y., Li, X., Sun, R., Kljun, N., Zhang, L., Wang, X., Zhu, G., 2016. Spatial representativeness and uncertainty of eddy covariance carbon flux measurements for upscaling net ecosystem productivity to the grid scale. Agric. For. Meteorology 230-231, 114—127.

Rinne, J., Riutta, T., Pihlatie, M., Aurela, M., Haapanala, S., Tuovinen, J.P., Tuittila, E.S., Vesala, T., 2007. Annual cycle of methane emission from a boreal fen measured by the eddy covariance technique. Tellus Ser. B-chemical Phys. Meteorology 59, 449—457.

Rochette, P., Gregorich, E., Desjardins, R., 1992. Comparison of static and dynamic closed chambers for measurement of soil respiration under field conditions. Can. J. Soil Sci. 72, 605—609.

Rodhe, H., 1990. A comparison of the contribution of various gases to the green-house effect. Science 248, 1217—1219.

Roulet, N.T., Rosemary, A., Moore, T.R., 1992. Low Boreal wetlands as a source of atmospheric methane. J. Geophys. Res. Atmos. 97, 3739—3749.

Schuur, E.A.G., Bockheim, J.C., Josep, G., Euskirchen, E., Field, C.B., Goryachkin, S.V., Hagemann, S., Kuhry, P., Lafleur, P.M., Lee, H., Mazhitova, G., 2008. Vulnerability of permafrost carbon to climate change: implications for the global carbon cycle. Bioscience 58, 701—714.

Song, C., Xiaofeng, X.U., Tian, H., Wang, Y., 2009. Ecosystem—atmosphere exchange of CH_4 and N_2O and ecosystem respiration in wetlands in the Sanjiang Plain, Northeastern China. Glob. Change Biol. 59, 692—705.

Song, C., Xu, X., Sun, X., Tian, H., Sun, L., Miao, Y., Wang, X., Guo, Y., 2012. Large methane emission upon spring thaw from natural wetlands in the northern permafrost region. Environ. Res. Lett. 7, 34009—34016 (34008).

Song, W., Wang, H., Wang, G., Chen, L., Jin, Z., Zhuang, Q., He, J.S., 2015. Methane emissions from an alpine wetland on the Tibetan Plateau: neglected but vital contribution of the nongrowing season. J. Geophys. Res. Biogeosciences 120, 1475—1490.

Sonnentag, O., Kamp, G.V.D., Barr, A.G., Chen, J.M., 2010. On the relationship between water table depth and water vapor and carbon dioxide fluxes in a minerotrophic fen. Glob. Change Biol. 16, 1762—1776.

Sorrell, B.K., Boon, P.I., 1994. Convective gas flow in *Eleocharis sphacelata* R. Br.: methane transport and release from wetlands. Aquat. Bot. 47, 197—212.

Ström, L., Tagesson, T., Mastepanov, M., Christensen, T.R., 2012. Presence of Erio-phorum scheuchzeri enhances substrate availability and methane emission in an Arctic wetland. Soil Biol. Biochem. 45, 61—70.

Sun, X.-M., Zhu, Z.-L., Wen, X.-F., Yuan, G.-F., Yu, G.-R., 2006. The impact of averaging period on eddy fluxes observed at ChinaFLUX sites. Agric. For. Meteorology 137, 188—193.

Suyker, A.E., Verma, S.B., Clement, R.J., Billesbach, D.P., 1996. Methane flux in a boreal fen: season-long measurement by eddy correlation. J. Geophys. Res. Atmos. 101, 28637—28647.

Tagesson, T., Mölder, M., Mastepanov, M., Sigsgaard, C., Tamstorf, M.P., Lund, M., Falk, J.M., Lindroth, A., Christensen, T.R., Ström, L., 2012. Land-atmosphere exchange of methane from soil thawing to soil freezing in a high-Arctic wet tundra ecosystem. Glob. Change Biol. 18, 1928—1940.

Updegraff, K., Bridgham, S.D., Pastor, J., Weishampel, P., Harth, C., 2001. Response of CO_2 and CH_4 emissions from peatlands to warming and water table manipulation. Ecol. Appl. 11, 311—326.

Vickers, D., 1997. Quality control and flux sampling problems for tower and aircraft data. J. Atmos. Ocean. Technol. 14, 514—526.

Wang, X., Li, X., Hu, Y., Lv, J., Sun, J., Li, Z., Wu, Z., 2010. Effect of temperature and moisture on soil organic carbon mineralization of predominantly permafrost peatland in the Great Hing'an Mountains, Northeastern China. J. Environ. Sci. 22, 1057—1066.

Webb, E.K., Pearman, G.I., Leuning, R., Webb, E.K., Pearman, G.I., Leuning, R., 1980.

Correction of flux measurements for density effects due to heat and water-vapor transfer. Q. J. R. Meteorological Soc. 106, 85–100.

Weiss, R., Shurpali, N.J., Sallantaus, T., Laiho, R., Laine, J., Alm, J., 2006. Simulation of water table level and peat temperatures in boreal peatlands. Ecol. Model. 192, 441–456.

Whalen, S.C., Reeburgh, W.S., 1992. Interannual variations in tundra methane emission: a 4-year time series at fixed sites. Glob. Biogeochem. Cycles 6, 139–159.

Whiting, G.J., Chanton, J.P., 1992. Plant-dependent CH_4 emission in a subarctic Canadian fen. Glob. Biogeochem. Cycles 6, 225–231.

Wille, C., Kutzbach, L., Sachs, T., Wagner, D., Pfeiffer, E.M., 2008. Methane emission from Siberian arctic polygonal tundra: eddy covariance measurements and modeling. Glob. Change Biol. 14, 1395–1408.

Wuebbles, D.J., Hayhoe, K., 2002. Atmospheric methane and global change. Earth-Science Rev. 57, 177–210.

Zhang, Y., Li, C., Trettin, C.C., Li, H., Sun, G., 2002. An integrated model of soil, hydrology, and vegetation for carbon dynamics in wetland ecosystems, 9–1-9-17 Glob. Biogeochem. Cycles 16.

Zhu, R., Ma, D., Xu, H., 2014. Summertime N_2O, CH_4 and CO_2 exchanges from a tundra marsh and an upland tundra in maritime Antarctica. Atmos. Environ. 83, 269–281.